J Mater Sci (2010) 45:5398–5405
DOI 10.1007/s10853-010-4592-3

Applicability of the polymeric precursor method to the synthesis of nanometric single- and multi-layers of $Zn_{1-x}Mn_xO$ ($x = 0$–0.3)

J. Mera · C. Córdoba · J. Benavidez · O. Paredes · J. Doria · A. Gómez · C. Sanchez · C. Paucar · O. Morán

Received: 26 November 2009 / Accepted: 4 May 2010 / Published online: 19 May 2010

Abstract Polymeric precursor method (Pechini) was employed to fabricate single- and multilayers of $Zn_{1-x}Mn_xO$ ($x = 0$–0.3) on glass substrates. X-ray diffraction measurements revealed that crystal structure of $Zn_{1-x}Mn_xO$ multilayers is the typical hexagonal würzite structure of pristine ZnO. A reduced peak intensity and widened full width half maximum (FWHM) value of prominent peaks suggested that the Mn^{2+} ions have substituted the Zn^{2+} ion without changing the würzite structure of pristine ZnO up to Mn concentrations $x \leq 0.2$. A distinct redshift of the absorption edge was observed as the Mn concentration x was increased. Additionally, the absorption edge was less sharp due, probably, to *s–d* and *p–d* interactions, which give rise to band gap bowing. Nevertheless, amorphous states appearing in the band gap as a consequence of reduced crystallinity may also be responsible for the shrinking of the band gap in this material. Interestingly, the field dependence of the magnetization showed typical paramagnetic behavior for all the chosen Mn concentrations with no evidence of ferromagnetic ordering. Probably, the absence of ferromagnetism in the studied $Zn_{1-x}Mn_xO$ films is strongly related to defects (say Mn impurities at the interface between nano-crystallites) in ZnO due to partial substitution of host Zn ions by Mn ions.

J. Mera · C. Córdoba · J. Benavidez · O. Paredes
Centro de Investigaciones en Materiales, Facultad de Ingeniería, Universidad de Nariño, Ciudad Universitaria Torobajo, Pasto, Colombia

J. Doria (✉) · C. Sanchez · C. Paucar · O. Morán
Laboratorio de Materiales Cerámicos y Vítreos, Departamento de Física, Universidad Nacional de Colombia, sede Medellín, A.A. 568, Medellín, Colombia
e-mail: jgdoria@unal.edu.co

A. Gómez
Departamento de Ingeniería de Materiales, Universidad Nacional de Colombia, sede Medellín, A.A. 568, Medellín, Colombia

Introduction

Transparent conducting oxides are basic materials for novel applications in various fields of optical and electronic devices [1, 2]. Recent theoretical studies claiming the existence of a ferromagnetic ground state in substituted ZnO have opened new expectations for technological applications of this oxide [3] which base on a possible magnetic control of the optical and electrical properties [4]. Certainly, great interests in spintronic devices which pursue the dream of using spin degree of freedom of the charge charier so as to increase both speed and storage capacity in microelectronic devices has stimulated the investigation of dilute magnetic semiconductors (DMS) with promising magnetic properties [5, 6]. DMS materials involve the charge of semiconductors (where spin is inactive) and the spin of the magnetic dopants in a single substance. Hence, the physics of them is specially traced on the functionality of magneto-optic devices. The finding of room temperature ferromagnetism in some thin films seemed to verify previous theoretical predictions [7], although several studies have thrown doubts on the intrinsic nature of the magnetic behavior [8]. Among the potential candidates to DMS, the wide band gap ZnO has received considerable attention due to the possibility of partially substituting Zn^{2+} ions by magnetic ions in the hexagonal structure [3]. The band gap of ZnO amounts to $\sim$3.3 eV at room temperature and the crystals are unintentionally n-type [9]. Physical methods as sputtering or pulsed laser deposition have been extensively used for the preparation of ZnO films [10–13]. The two mentioned

methods normally use targets from which the films are ablated or sputtered. The targets are fabricated by pressing powders which are commonly synthesized by standard solid state reaction. The main difficulty with this synthesis (solid state reaction) is the lack of uniformity in the fine particle distribution due to the abnormal crystal growth at high temperatures. On the other hand, the synthesis of oxides using soft chemistry methods such as sol–gel or chemical coprecipitation has demonstrated to be effective in getting nanometric sized particles with uniform particle size distribution [14]. The lower processing temperatures required by these synthesis methods seem to play an important role in achieving oxides with these characteristics [15]. In the sol–gel technology, there are several methods of preparation which depend on the employed metal alcoxides [16]. Some methods are more versatile than others and involve determined organometallic compounds in an alcoholic dissolvent followed by a series of chemical reactions of hydrolysis, condensation, and curing to produce a gel which is formed by a continuous inorganic network [17]. The most important step in this route is the formation of an inorganic polymer by means of hydrolysis reactions. The hydrolysis of a solution like tetraethyl orthosilicate (TEOS) in a dissolvent as ethanol allows for the formation of silanols groups which form a sol. A gel is then obtained by a molecular cross-linking through the curing by subsequent condensation [18]. Although the main disadvantage of this wet chemical synthesis is the lack of information related to the involved chemical reactions during the formation of the complexes, this has not prevented that the method to be widely used for the synthesis of multicomponent oxide to diverse applications [19].

In this work, the successful growth of $Zn_{1-x}Mn_xO$ ($x = 0$–0.3) multilayers on glass substrates using the polymeric precursor method (Pechini) is reported. Remarkable experimental results as the absorption edge shift (observed by UV–Vis spectroscopy) along with the absence of ferromagnetism in the temperature range 300–5 K for all Mn doping levels are discussed in detail.

Experiment

The preparation of the coating solutions is based on the Pechini method [20]. $Zn(CH_3CO_2)_2{\cdot}2H_2O$ dihydrate (Fluka, 99.5%) and $Mn(CH_3CO_2)_2{\cdot}4H_2O$ tetrahydrate (Aldrich 99%) were used as starting precursors. *N*,*N*-dimethylformamide (Fisher 99%) was employed as dissolvent. Zinc acetate dihydrate and manganese acetate tetrahydrate were dissolved in *N*,*N*-dimethylformamide (concentration: 0.6 M) at room temperature under permanent stirring. The molar ratio of Zn to Mn was 0.94:0.06. The resulting solution was stirred up to yielding a clear and homogeneous sol which served as the coating material. In case of the pristine ZnO films, zinc acetate dihydrate was first dissolved in ethanol at room temperature (concentration: 0.6 M). The solution was subjected to reflux for 2 h at 60 °C and then triethanolamine (Merck, 99%), in a molar ratio to zinc acetate of 6:5, was added as stabilizer. The solution was stirred for 30 min at 60 °C in order to get a clear and homogeneous solution which served as the precursor solution. At this stage, it was observed that the time needed to get the appropriated coating solution was less than that involved in the traditional sol–gel procedure (sometimes more than 24 h) [21]. Previous to the coating, the glass substrates were treated with a standard wet cleaning procedure. The $Zn_{1-x}Mn_xO$ ($x = 0$–0.3) films were prepared from the precursor solution using the spin-coating method. After setting the glass substrate on the disk of the spin-coater, the coating solution (approx. 0.2 mL) was dropped and spin-coated at 3000 rpm for $\sim$20 s in air. After each spin coating, the substrates were heated at 80 °C for 10 min in an open-air oven. The process from coating to drying was repeated several times in order to achieve the desired thickness of the $Zn_{1-x}Mn_xO$ multilayer. Finally, the coated substrates were heated at 500 °C for 1 h. The crystal structure of the films was analyzed by X-ray diffraction (XRD) at room temperature in standard θ-2θ configuration. The surface of the films was analyzed by scanning electron microscope (SEM) operating at 7 kV. Elemental analysis was carried out by energy-dispersive X-ray spectroscopy (EDS). The optical properties of the films were characterized by recording the UV–VIS absorption spectra using an Ocean optics spectrophotometer (wavelength range 200–900 nm). Complementary Raman scattering measurements were performed on a microlaser Raman system (JY instruments) at backscattering geometry using a 623 nm laser as excitation source. The magnetic response of the blank substrates and $Zn_{1-x}Mn_xO$ ($x = 0$–0.3) films was detected by sensible measurements of the magnetization as a function of the field using a Quantum Design SQUID magnetometer.

Results and discussion

Displayed in Fig. 1a is the XRD pattern measured on a representative ZnO multilayer formed by a 10-cycle spin-coating of the glass substrate. Solid lines correspond to experimental data and symbols to Rietveld refinement. The analysis of the XRD pattern indicates that the ZnO film is single phase with würtzite crystal structure of ZnO (space group $P6_3mc$). No additional peaks corresponding to any secondary crystalline phase (e.g., unreacted MnO_2) were detected for this sample. Nevertheless, this does not preclude the presence of secondary phases since X-ray

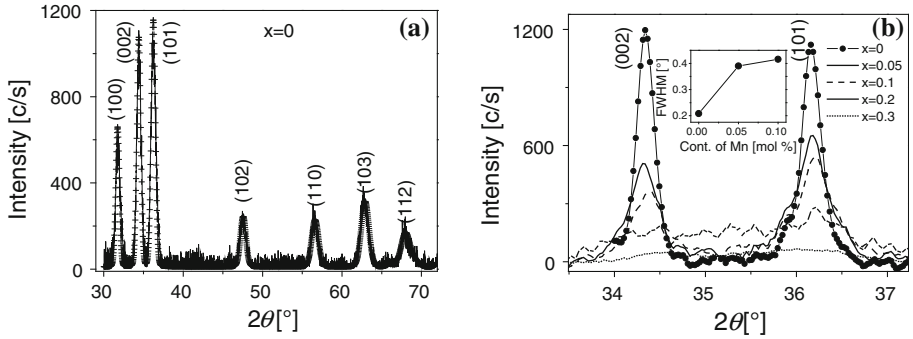

Fig. 1 **a** X-ray diffraction pattern (experimental data as *solid line* and Rietveld simulation as *crosses*) of an undoped ZnO film grown on a glass substrate at 500 °C by polymeric precursor method. **b** XRD pattern of $Zn_{1-x}Mn_xO$ ($x = 0$, 0.05, 0.1, 0.2, and 0.3) films deposited on glass substrates at 500 °C. Inset: FWHM of the $Zn_{1-x}Mn_xO$ films plotted in the main panel

diffraction, being a "bulk" technique, is not always sensitive to small precipitates of a secondary phase especially for low level of doping. More sophisticated techniques as NEXAFS may give more convincing information about the degree of purity of the compound. The addition of Mn certainly alters the diffraction angle (shift to lower angles), the peak intensity and the full width half maximum (FWHM) value of prominent peaks as the (002) suggesting the incorporation of Mn ions in the Zn lattice (Fig. 1b). The crystalline size of the films has been determined by Scherrer's formula using the XRD line broadening method [22]. Here, the crystal size $D = 0.9\lambda/(B \cdot \cos\theta)$, where λ represents the wavelength of the X-ray radiation, B the FWHM value and θ the diffraction angle. The estimated average crystalline sizes are ~40, ~22, and 20 nm for the Mn concentration 0, 0.05, and 0.1%, respectively. Inset to Fig. 1b shows the variation of FWHM of the (002) peak as a function of Mn concentration. It is observed that the increase in Mn concentration increases the FWHM reducing thus the grain size and increasing the grain boundaries in the films. Such effect ultimately leads to reduced crystallinity. Here, it is understood that more Mn ions have been incorporated in the Zn lattice site. Probably, the increase in the Mn concentration would enhance the nucleation of the ZnO phase resulting in a smaller grain size [23]. Note that for Mn concentrations $x > 0.1$, the crystallinity of the films quickly decreases becoming practically amorphous for $x > 0.2$. On the other hand, the c-axis lattice constant of $Zn_{1-x}Mn_xO$ films as obtained by Rietveld refinement increased from 5.205 Å for $x = 0$, 5.216 Å for $x = 0.02$ and 5.258 Å for $x = 0.05$. Since the ionic radius of Zn^{2+} (0.74 Å) is smaller than that of Mn^{2+} (0.80 Å) and larger than that of Mn^{3+} (0.66 Å), the increase of the c-axis lattice parameter with the Mn doping indicated that the divalent Mn^{2+} ions substituted for Zn^{2+} ions in ZnO crystal lattice [24]. The latter results suggest that Mn atoms substitute for Zn sites in the films fabricated by Pechini's method without changing the würzite structure ($x \leq 0.2$).

Figure 2a shows a SEM micrograph of the surface of a $Zn_{0.95}Mn_{0.05}O$ multilayer prepared by repeating the spin-coating ten times and preheat-treatment at 80 °C and by post-heating at 500 °C. The image gives a general view of the morphology of the so fabricated ZnO multilayer. Crystallites of different lateral sizes may be found. The top-flat crystallites with hex-like shape suggest the würzite structure. On the facets of these relative big crystallites a number of small holes may be seen. The corresponding EDS spectrum of this sample is presented in Fig. 2b. The analysis of the chemical composition of this sample showed consistency with the molar ratio of $Zn_{0.95}Mn_{0.05}O$. EDS mapping was carried out on a large area of the films encountering similar spectra. This finding speaks for a chemically homogeneous coating of the glass substrates by the coating solution.

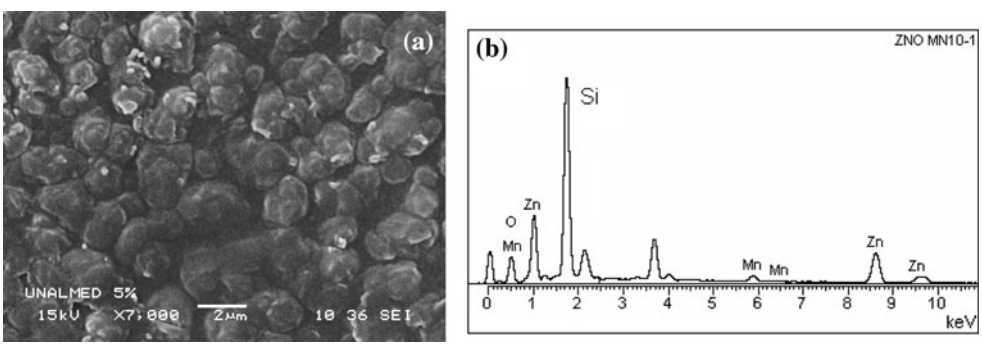

Fig. 2 SEM image (**a**) and corresponding EDS spectrum (**b**) of a typical $Zn_{0.95}Mn_{0.05}O$ film deposited on a glass substrate polymeric precursor method

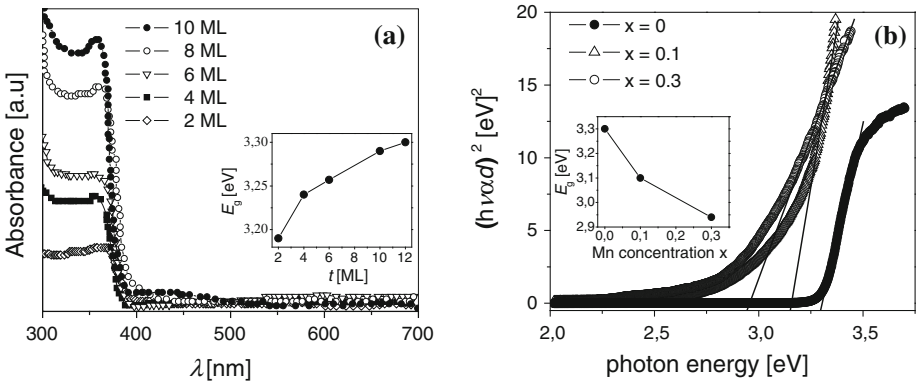

Fig. 3 **a** Room temperature absorption spectra in the wavelength for ZnO films with various thicknesses (*ML*). Inset: Variation of the energy gap (E_g) of ZnO films as a function of the thickness t given in ML. **b** $(\alpha hvd)^2$ as a function of the photon energy for ZnO multilayers with different Mn concentrations. The *solid lines* represent the straight part of the curve used to calculate the energy gap E_g. Inset: variation of E_g with the Mn concentration x

The room temperature absorption spectra in the wavelength (λ) range of 300–700 nm for pristine ZnO films with various thicknesses are shown in Fig. 3a. The increase of the number of the deposited layers resulted in the higher absorption of samples. Interestingly, a progressive formation of the exciton band at 356 is clearly observed on this plot. This band being practically absent in the 2- and 4-layer samples appears starting with thicknesses larger than 6 layers. The absorption spectra featured transparency in the visible range ($\lambda > 400$ nm) larger than 90% and a sharp ultraviolet absorption edge at $\lambda \sim 380$ nm. These characteristics are typical for high quality ZnO films [25, 26]. Indeed, the high transmittance displayed by these films suggests low optical scattering associated with uniformity of the particle size distribution. Similar measurements were carried out on Mn-doped ZnO multilayers. Based on measured absorbance spectra, the band gap energy, E_g, of these samples was determined. Theory of optical absorption gives the relationship between the absorption coefficients α and the photon energy hv for direct allowed transition as $(\alpha hv)^2 = B(hv - E_g)$ where B represents a constant which depends on density of states. The direct band gap may be determined using the last equation when the straight portion of the $(\alpha hv)^2$ vs. hv plot is extrapolated to intersect the energy axis at $\alpha = 0$ (Fig. 3b). The value of band gap was found to decrease from 3.1 to 2.94 eV with corresponding increase in Mn concentration ($x = 0$–0.3), respectively, as it is shown in inset of Fig. 3b. Additionally, the absorption edge was observed to be less sharp which is probably due to Mn states extending into the band gap. Commonly, the observed decrease in the band gap has been explained invoking a *sp–d* exchange interaction, i.e., manifestation of strong exchange interaction present between *d* electron of Mn, and the *s* and *p* electrons of host matrix [27]. The main *d–d* transitions occur at $^6A_1 \rightarrow {}^4T_1$, $^4T_2$, $^4A_1$, ^4E energy levels of Mn^{2+} ion in the presence of tetrahedral crystal field interaction [28]. Although exchange interaction is especially important in the presence of an external magnetic field H, in certain cases it may manifest at $H = 0$. An alternative explanation of the E_g shrinkage and, probably, the most consistent with the achieved results on the films reported in the present work shall take into account amorphous states appearing in the band gap. As it is evident from the XRD patterns, the crystallinity of the films diminishes with the possible incorporation of Mn ions into the Zn lattice. A diminished crystallinity leads to more amorphous states appear in the band gap causing the band gap to shrink. It is found, as a general rule, that the band-edge and the near band-edge regime are very sensitive to the epitaxial relationship between the films and the substrate, the strains in the films and in particular to the microstructure achieved in each case. Crystallographic misfit at the boundary between the misoriented grains results in intrinsic lattice defects (primary and secondary dislocations dangling bonds, bond bending and fluctuations of bond angles), as well as in extrinsic electronic defects due to a preferential segregation of impurities and doping atoms at the grain boundary. These extrinsic and intrinsic defects introduce states into the forbidden gap which act as traps and recombination centers. Tail states have been detected at grain boundaries in bicrystals [29] as well as in fine-grained films [30] of diverse semiconductors. At ideal interfaces without broken or distorted bonds there are no states within the forbidden gap of semiconductors as Si. Broken bonds result, however, in midgap states [31]. It is speculated that band tails in disordered semiconductors generally arise from short-wavelength potential fluctuations due to spatial disorder; these quantum well fluctuations localize free carriers. Because of the small grain sizes realized in films produced by soft chemistry methods (this work) and the lower carrier concentration within the grains (the films are highly

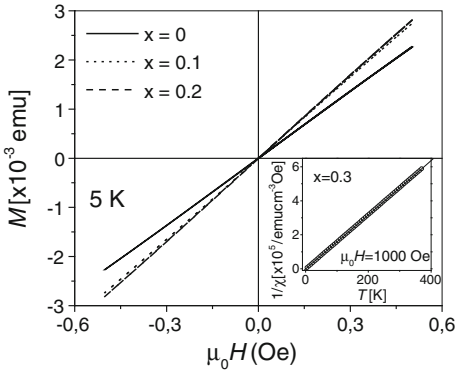

Fig. 4 Field-dependent magnetization of $Zn_{1-x}Mn_xO$ ($x = 0$–0.2) multilayers recorded at 5 K. Inset: Inverse magnetic susceptibility ($1/\chi$) as a function of temperature for a $Zn_{0.7}Mn_{0.3}O$ film measured in an external field of 1000 Oe

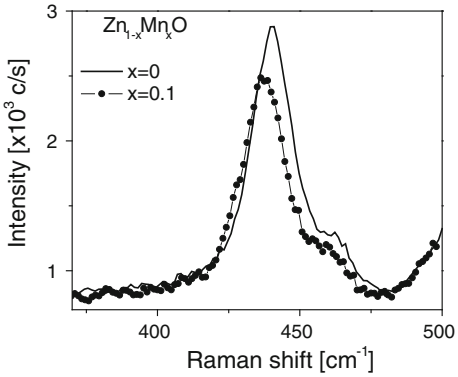

Fig. 5 Raman spectra of $Zn_{1-x}Mn_xO$ ($x = 0$ and 0.1) films on glass substrates

resistive), a substantial portion of the grains are depleted and a flat band description is no longer appropriate. Instead, the potential varies throughout most of the grains. The varying electrostatic potential results in electric fields at the grain boundaries which, is proposed, may cause optical transitions between the highest point of the valence band and the lowest point of the conduction band thereby altering the optical absorption edge [32]. Aside from the redshift observed in the investigated films, overall blue shift of the band gap with increase in Mn concentration has also been observed in thin films of Mn-doped ZnO fabricated using diverse methods and the reason for blue shift was attributed to the higher band gap energy of MnO (4.2 eV) [33, 34].

The field dependence of the zero-field-cooled (ZFC) magnetization of $Zn_{1-x}Mn_xO$ ($x = 0$–0.2) multilayers (0.5×0.5 cm^2) grown on glass substrates was measured at 5 K in the magnetic field range of ± 0.6 T (Fig. 4). The experimental data were corrected for the diamagnetic contribution due to the background signal from glass substrate. A perfect linear $M(H)$ behavior (even down to very low fields) is clearly observed for all the Mn concentrations. The linear dependence of M on H indicates that the samples are paramagnetic even at very low temperatures. The slight increase in the value of the susceptibility (M/H) with Mn concentration indicates that the number of Mn ions in ZnO lattice is increased which agree well with the XRD patterns. This finding is in contrast to some reports on $Zn_{1-x}Mn_xO$ ($x = 0.02$) films prepared under relatively low temperature conditions [28] in which evidence for ferromagnetic order at room temperature was found. The origin for this discrepancy is unclear although there are suggestions that these earlier measurements were sensitive to unreacted manganese oxides. Even where the temperature of synthesis is relatively low, some of the synthetic procedures are not convincing as to whether the dopant has substituted the Zn site. Furthermore, the magnetization values reported by many workers resulted to be very low and may arise from the presence of magnetic impurities which cannot be detected by X-ray diffraction. It has also been shown that the secondary phase $Mn_{2-x}Zn_xO_{3-\delta}$, or an extrinsic source, is responsible for ferromagnetism in Mn-doped ZnO which was initially thought to be intrinsic [1]. In the case of $Zn_{1-x}Mn_xO$ thin films synthesized by polymeric precursor method technique (this work), the constituent elements were mixed at molecular level ensuring dopant atoms are present at substitutional sites as inferred from XRD and optical measurements on these films. Moreover, the deposition temperature was kept relatively low to avoid any possible impurity phase segregation even at relatively high doping levels. Although Pechini process may provide excellent control over dopant speciation and allow effective isolation and purification of the desired products, it is evident that partial substitution of nonmagnetic host ions by dopant ions may result in many defects and lattice disorder in the host semiconductor [35]. Comprehensive study of defects and lattice disorder in host semiconductors may decidedly help to understand the origin of ferromagnetism in DMS [36]. As paramagnetism may be related to the destruction of ZnO caused by Mn clusters and defects (not easily detected in films with usual XRD) [37], Raman scattering was used to explore the presence of defects and lattice disorder induced by Mn dopants. Indeed, Raman scattering is a versatile technique for fast and nondestructive study of dopant incorporation and its resulting defects and lattice disorder in host lattice [35]. The room temperature Raman spectra of $Zn_{1-x}Mn_xO$ ($x = 0$ and 0.1) films on glass substrates recorded around the sharpest and strongest peak at about 437 cm^{-1} are shown in Fig. 5. This peak may be assigned to the high frequency branch of E_2 mode [E_2 high] of ZnO which is the strongest mode in würzite crystal structure [38]. The values of FWHM of E_2 (high) mode are 16.34 ($x = 0$) and 18.14 cm^{-1} ($x = 0.1$), respectively, which suggest that

$Zn_{1-x}Mn_xO$ ($x \leq 0.1$) films keep still a good würzite ZnO structure. The Raman scattering results are well consistent with those of XRD. However, the widening and weakening of the Raman line of E_2 of the doped film indicates that the ZnO crystal structure is indeed affected at this Mn concentration. At higher Mn concentrations, the Raman line of E_2 becomes very broad and weak which is similar to that of amorphous ZnO. The increasing deformation (and final collapse) of the ZnO crystal structure may be caused by the formation of Mn clusters and generation of defects such as vacancies and interstitials (not easily detected by normal XRD measurements). It is apparent that in the $Zn_{1-x}Mn_xO$ films (this work) host ZnO ions are partially substituted by Mn ions, which introduces lattice defects and disorder in host ZnO. These lattice defects and disorder disrupt the long range ionic ordering in the ZnO [35]. Such a disruption may weaken the electric field associated with the E_2 mode shifting then its frequency to lower values (Fig. 5). The connection between defects and magnetism has been thought to be an important factor for the room temperature ferromagnetism in DMS [39, 40]. Schwarz and Gamelin [39] reported that the room temperature ferromagnetic ordering in Co^{2+}:ZnO could be switched between "on" and "off" when introducing or removing defects of ZnO. Raman scattering studies by Wang et al. [35] clearly showed that defects in $Zn_{1-x}Mn_xO$ nanoparticles (synthesized by ultrasonic assisted sol–gel process) increase with the increment of Mn content. Whereas increasing dependence of ferromagnetic ordering (at 350 K) on Mn content ($x \leq 0.02$) was observed, samples doped with 5% Mn only showed paramagnetism. These authors concluded that defects are an important factor affecting the room temperature ferromagnetism as the ZnO structure in $Zn_{1-x}Mn_xO$ ($x = 0.05$) nanoparticles was practically destroyed. In an interesting work, Coey et al. [41] pointed out that ferromagnetic exchange in diluted ferromagnetic oxides may be mediated by shallow donor electrons. Hence, it was presumed that the role of defects in $Zn_{1-x}Mn_xO$ nanoparticles is shallow donors. As it was pointed earlier, the collapse of the ZnO structure in $Zn_{1-x}Mn_xO$ nanoparticles may be caused by the formation of Mn clusters because of the low solubility of Mn in ZnO. Sharma et al. [42] observed that Mn clusters may suppress the ferromagnetism, and a large paramagnetic effect was observed in $Zn_{1-x}Mn_xO$ nanoparticles. The latter results gave to understand that besides the defects in transition-metal-doped ZnO, a correct doping concentration is crucial for making a viable ferromagnetic DMS. So, the paramagnetism observed in the Mn-doped ZnO nano-crystalline films grown by Pechini's method might be caused Mn impurities (formed on the interface between nano-sized crystallites) which may be not easily detected by standard RXD measurements. On the other hand, theoretical work has demonstrated that robust ferromagnetism is not obtained by substitution of Co or Mn on the Zn site, unless additional carriers (holes) are also incorporated [43]. This result is consistent with the conventional wisdom that carriers are required to induce ferromagnetism in diluted magnetic semiconductors. The large body of literature on other diluted magnetic semiconductors concludes that carriers are required to mediate the ferromagnetism. For Mn substitution they predicted that hole doping would induce ferromagnetism [44]. In order to proof this statement, the evolution of carrier density and Fermi energy level with the Mn concentration (x) should be determined experimentally. This information may shed light on the reason for the absence of ferromagnetism in the films as the ferromagnetism in DMS depends on carrier density and Fermi level [41]. The change of Fermi level changes the configuration of Mn ions, which will directly affect the magnetic property observed for the material [45]. The carrier density and the Fermi level may be experimentally estimated by Hall effect and electrochemical [capacitance–voltage (C–V)-characteristics of a film/electrolyte junction] measurements, respectively. The presence of anomalous Hall coefficient (AHE) has been considered as one of the strong evidences for intrinsic ferromagnetism in DMS [46, 47]. However, considering the fact that AHE has also been reported in ferromagnetic clusters [48], granular materials [49], and inhomogeneous DMS in the hopping transport regime [50], observation of AHE alone cannot support the claim that the DMS under study is a ferromagnet of intrinsic origin, unless it is correlated with ferromagnetism observed by other means and furthermore, secondary phases and precipitates must be absent in the sample. $Zn_{1-x}Mn_xO$ ($x = 0.006, 0.072, 0.18, 0.21$) films grown by the MOCVD technique have been electrically characterized by Hall effect measurements [51]. The results showed n-type carrier concentrations of the order of 10^{18} cm^3 for all samples, while mobility decreased with increasing manganese content from 186 to 6.64 cm^2/V s. Since Mn^{2+} is an isovalent impurity in ZnO compound, no change in the carrier concentration may be expected. Although Hall effect and C–V-measurements on the nano-crystalline $Zn_{1-x}Mn_xO$ films reported in the present work are still lacking, it is probable that the carrier transport and in particular the Hall analysis to be governed by the properties of the grain boundaries. Certainly, the grain boundaries may be limiting factor for the mobility in the layers as they may act as potential barriers and scattering centers. In this case, Hall analysis would be no good measure of the material parameters. C–V-measurements using, for instance, an Hg-prober to implement Schottky contacts on the films might be used instead. Nevertheless, in order to understand in more detail the effect of Mn on electron mobility, temperature-dependent measurements shall be performed.

Conclusions

Multilayers of the semiconducting $Zn_{1-x}Mn_xO$ with different doping concentration were successfully grown on glass substrates by polymeric precursor method at relatively low temperature. This method allowed for mixing the starting precursors at atomic level reducing thus the possibility of formation of Mn impurity phases. Although, the analysis of the XRD pattern indicated that the $Zn_{1-x}Mn_xO$ ($x < 0.2$) films were single phase with würtzite crystal structure of ZnO, the presence of Mn impurities and defects may not be precluded. The structural and optical properties measured on these films suggested that the Mn^{2+} ions have partially substituted the Zn^{2+} ion without changing the würtzite structure of pristine ZnO. Although the würtzite crystal structure was maintained, the incorporation of Mn may lead to a large amount of structural disorder in the crystalline columnar ZnO lattice. The observed decrease in the energy band gap with increase in Mn concentration may be explained by amorphous states appearing in the band gap as consequence of reduced crystallinity of the doped ZnO films. No evidence of ferromagnetic ordering was observed for all the considered Mn concentrations. Probably, the presence of Mn clusters and defects, due to the high doping concentrations, plays a decisive role into the observed paramagnetism. The controversy between research teams may result from the growth method used and/or from the growth conditions. In fact, depending on the different growth modes and mechanisms, microstructures in these systems such as distribution of Mn ion in ZnO crystal lattice and the local environment around Mn ions may be very different, which considerably affects the magnetic properties.

Acknowledgements This work was supported by Vicerrectoría de investigaciones de la Universidad de Nariño (Contract 113, 19.05.09) and Universidad Nacional de Colombia, sede Medellín (Contract 20101007305). O. M. acknowledge also the financial support of the German Academic Exchange Service (DAAD) through the program "Wiedereinladung".

References

1. Blasco J, Bartolomé F, García LM, García J (2006) J Mater Chem 16:2282
2. Matsuda A, Akiba S, Kasahara M, Watanabe T, Akita Y, Kitamoto Y, Tojo T, Kawaji H, Atake T, Koyama K, Yoshimoto M (2008) Thin Solid Films 516:3873
3. Dietl T, Ohno H, Matsukura F, Cibert J, Ferrand D (2000) Science 287:1019
4. Sato K, Katayama-Yoshida H (2001) Jpn J Appl Phys 40:L334
5. Mandal SK, Das AK, Nath TK, Karmakar D, Satpati B (2006) J Appl Phys 100:104315
6. Miah MI, Gray EM (2008) Solid State Sci 10:205
7. Venkatesan M, Fitzgerald CB, Lunney JG, Coy M (2004) Phys Rev Lett 93:77206
8. Kim JH, Kim H, Kim D, Ihm Y, Choo WR (2004) J Eur Ceram Soc 24:1847
9. Muth JF, Kolbas RM, Sharma AK, Oktyabrsky S, Narayan J (1999) J Appl Phys 85:7884
10. Elanchezhiyan J, Bhuvana KP, Gopalakrishnan N, Balasubramanian T (2008) Mater Lett 62:3379
11. Elanchezhiyan J, Bhuvana KP, Gopalakrishnan N, Balasubramanian T (2008) J Alloys Compd 463:84
12. Pivin JC, Soco G, Mihailescu I, Berthet P, Singh F, Patel MK, Vincent L (2008) Thin Solid Films 517:616
13. Smolentsev N, Soldatov AV, Smolentsev G, Weib SQ (2009) Solid State Commun 149:1803
14. Yoon SH, Liu D, Shen D, Park M, Kim D-J (2008) J Mater Sci 43:6177. doi:10.1007/s10853-008-2929-y
15. Natsume Y, Sakata H (2000) Thin Solid Films 372:30
16. Segal D (1997) J Mater Chem 7:1297
17. Yang Z, Liu Q-H (2008) J Mater Sci 43:6527. doi:10.1007/s10853-008-2852-2
18. Nanto H, Sokooshi H, Kawai T, Usuda T (1992) J Mater Sci Lett 11:235
19. Liu Y, Yang S-H, Zhang Y-L, Bao D-H (2009) J Magn Magn Mater 321:3406
20. Pechini MP (1967) U.S. Patent, No 3330697, 11 July 1967
21. Ohyama M, Kozuka H, Yoko T, Sakka S (1996) J Ceram Soc Jpn 104:296
22. Brus LE (1984) J Chem Phys 80:4403
23. Lin K, Tsai P (2007) Thin Solid Films 515:8601
24. Singh P, Kaushal A, Kaur D (2009) J Alloys Compd 471:11
25. Zhang DH, Brodie DE (1994) Thin Solid Films 238:95
26. Zhao JL, Lia XM, Bian JM, Yua WD, Gao XD (2005) J Cryst Growth 276:507
27. Alaria J, Bouloudenine M, Schmerber G, Colis S, Dinia A (2006) J Appl Phys 99:08M118
28. Senthilkumaar S, Rajendran K, Banerjee S, Chini TK, Sengodan V (2008) Mater Sci Semicond Process 11:6
29. Pike GE, Seager CH (1979) J Appl Phys 50:3414
30. Hirae S, Hirose M, Osaka Y (1980) J Appl Phys 51:1043
31. Laughlin RB, Joannopoulos JD, Chali DJ (1978) In: Pantilides ST (ed) The physics of SiO_2 and its interfaces. Pergamon, New York, p 321
32. Srikant V, Clarke R (1997) J Appl Phys 81:6357
33. Fukumura T, Jin Z, Ohtomo A, Koinuma H, Kawasaki M (1999) Appl Phys Lett 75:3366
34. Lin YB, Yang YM, Zhao GY, Chen W, Huang ZG (2010) Physica B 405:322
35. Wang JB, Huang GJ, Zhong XL, Sun LZ, Zhou YC (2006) Appl Phys Lett 88:252502
36. Hong NH, Sakai J, Huong NT, Poirot N, Ruyter A (2005) Phys Rev B 75:045336
37. Yang JH, Zhao LY, Zhang YJ, Wang YX, Liu HL, Wei MB (2007) Solid State Commun 143:566
38. Wang ZH, Geng DY, Zhang ZD (2009) Solid State Commun 149:682
39. Schwarz DA, Gamelin DR (2004) Adv Mater (Weinheim, Ger) 16:2115
40. Radovanovic PV, Gamelin DR (2003) Phys Rev Lett 91:157202
41. Coey JMD, Venkatesan M, Fitzgerald CB (2005) Nat Mater 4:173
42. Sharma P, Guptai A, Rao KV, Owens FJ, Sharma R, Ahuja R, Guillen JMO, Johansson B, Gehring GA (2003) Nat Mater 2:673
43. Spaldin NA (2004) Phys Rev B 69:125201
44. Sato K, Katayama-Yoshida H (2002) Phys Status Solidi B 229:673
45. Liu C, Yun F, Morkoc H (2005) J Mater Sci: Mater Electron 16:555
46. Ohno H, Shen A, Matsukura F, Oiwa A, Endo A, Katsumoto S, Iye Y (1996) Appl Phys Lett 69:363

47. Toyosaki H, Fukumura T, Yamada Y, Nakajima K, Chikyow T, Hasegawa T, Koinuma H, Kawasaki M (2004) Nat Mater 3:221
48. Shinde SR, Ogale SB, Higgins JS, Zheng H, Millis AJ, Kulkarni VN, Ramesh R, Greene RL, Venkatesan T (2004) Phys Rev Lett 92:166601
49. Sato H, Kobayashi Y, Aoki Y, Yamamoto Y (1995) J Phys Condens Matter 7:7053
50. Burkov AA, Balents L (2003) Phys Rev Lett 91:057202
51. Chikoidze E, Dumont Y, Jomard F, Ballutaud D, Galtier P, Ferrand D, Sallet V, Gorochov O (2006) Mater Res Bull 41:1038